Noninvasive technique for oximetry of blood in retinal vessels

François C. Delori

A noninvasive spectrophotometric technique for the measurement of oxygen saturation of the blood in discrete retinal vessels is described. The instrument, the retinal vessel oximeter, uses scanning fundus reflectometry to determine the optical density of a retinal vessel at three wavelengths (558, 569, and 586 nm). Oxygen saturation is determined after compensation for the effects of light scattering by the red blood cells by relating the measured densities with the corresponding extinction coefficients of oxyhemoglobin and deoxygenated hemoglobin. The vessel diameter is also measured continuously. All data acquisition and analysis are performed on-line by means of a microcomputer, and a vessel tracking system is used to compensate for the effects of eye movements. Oxygen saturation measurements for blood flowing through glass capillaries are presented as well as representative results of oxygen saturation measurements on normal human subjects.

I. Introduction

The oxygen supply of the retina is provided by both the choroidal and retinal circulation. The choroid serves as the oxygen source for the photoreceptors in the avascular outer retina, whereas the retinal circulation plays a critical role, mediated by its autoregulatory capacity, in maintaining the oxygen supply to the neural elements and nerve fibers in the inner retina. Because of the high oxygen needs of the retina (cerebral tissue), any alteration in circulation such as seen in diabetic retinopathy, hypertension, sickle cell disease, and vascular occlusive diseases results in functional impairment and extensive retinal tissue damage. Direct information on the oxygen supply to the retina in diseased and normal condition could be obtained from noninvasive measurements of blood flow and blood oxygen saturation (O_2Sat.) in retinal vessels. Although different optical methods have been developed to measure blood flow in retinal arteries and veins,[1–3] little instrumentation is presently available for determining the O_2Sat. of the blood in these vessels. Measurements of O_2Sat. in an artery and a vein of a vascular segment, combined with segmental blood flow measurements, permit an estimation of the rate of oxygen delivered to and metabolized by the retinal tissues.

Noninvasive measurement of the O_2Sat. of blood in retinal vessels was first proposed by Hickham *et al.*[4] using a two-wavelength (510- and 640-nm) photographic technique for retinal vessels crossing the optic disk. This method was used in conjunction with blood flow measurements in extensive studies of human retinal circulation.[5] Later Laing and co-workers[6–8] developed another two-wavelength (470- and 515-nm) photographic method and applied it to measurements of O_2Sat. in rabbits[8] and humans.[6] These methods were never reproduced, involved laborious microdensitometric analysis of photographic negatives obtained in controlled conditions, and did not lend themselves to large clinical studies or the study of rapid temporal changes. Furthermore, two-wavelength oximetry is based on the Lambert-Beer law and, therefore, strictly applies only to nonscattering hemolyzed blood. The effect of light scattering by the red blood cells (RBCs) in whole blood requires the introduction of a calibration procedure, which involves hazardous arterial puncture. Errors are introduced if one deviates from the calibration condition in respect to factors influencing light scattering, such as vessel diameter, hematocrit,[7] blood flow,[9] and fundus pigmentation.[6]

We developed a three-wavelength spectrophotometric technique[10] for oximetry of blood in retinal vessels and have previously reported on preliminary results.[11,12] Our approach is based on the three-wavelength method of Pittman and Duling[13] for transmission oximetry of whole blood with compensation for the effects of light scattering. We have adapted this method to retinal vessels and have developed a photo-

The author is with Eye Research Institute of Retina Foundation, 20 Staniford Street, Boston, Massachusetts 02114.

Received 26 June 1987.
0003-6935/88/061113-13$02.00/0.

electric system, the retinal vessel oximeter (RVO), that allows real-time measurements of O_2Sat. of discrete retinal vessels. In this paper we present the principles of the method, a description of the optical and electronic aspects of the RVO, results of *in vitro* experiments using blood flowing in glass capillaries, and typical results of O_2Sat. measurement on human retinal vessels.

II. Principles of Three-Wavelength Oximetry

Spectrophotometric oximetry methods are based on the fact that light absorption by blood depends on the blood oxygen saturation (O_2Sat.) and wavelength λ of light. Figure 1 shows the spectral variation of the specific extinction coefficient $E_{o,\lambda}$ of oxygenated hemoglobin (HbO_2) and of the coefficient $E_{r,\lambda}$ of deoxygenated hemoglobin (Hb).[14] The specific extinction coefficient E_λ of the mixture of the two pigments at a given O_2Sat. is given by

$$\begin{aligned} E_\lambda &= E_{o,\lambda} \cdot O_2\text{Sat.} + E_{r,\lambda} \cdot (1 - O_2\text{Sat.}) \\ &= E_{r,\lambda} + \Delta\lambda \cdot O_2\text{Sat.}, \end{aligned} \tag{1}$$

with $\Delta\lambda = E_{o,\lambda} - E_{r,\lambda}$. Oximetry is based on knowing the relationship between a measurable optical quantity such as optical density and the unknown E_λ. In this paper, we refer to the relationship between optical density D_λ and extinction E_λ as the D-E characteristic.

A. Transmission Oximetry of Whole Blood

For a layer of whole blood, the D-E characteristic for wavelengths between 500 and 600 nm was shown[13,15,16] to be of the following form:

$$D_\lambda = S + s.C.d \cdot (E_{r,\lambda} + \Delta\lambda \cdot O_2\text{Sat.}), \tag{2}$$

where C is the total hemoglobin concentration (in μmole/cm^3), and d is the path length (in centimeters). The wavelength-independent parameters S and s describe the influence of light scattering by RBCs and depend on d, the hematocrit, and the geometry of both the illumination and light collection optics. For complete collection of the transmitted light by an integrating sphere, Anderson and Sekelj[16] found $s = 1$, but values different from 1 were found using other geometries.[13,15] For hemolyzed blood ($S = 0$, $s = 1$), Eq. (2) becomes the Lambert-Beer law and is the basis of two-wavelength oximetry. With $E_{r,\lambda}$ and $\Delta\lambda$ known, density measurements at two wavelengths are needed to find the two unknowns: $C.d$ and O_2Sat.

Pittman and Duling's method for whole blood oximetry[13] is based on Eq. (2) and uses density measurements at three wavelengths to solve for the three unknowns S, the product $s.C.d$, and O_2Sat. Two isobestic wavelengths (520 and 546 nm) and one measuring wavelength (555 nm) are used. They verified their method[17] using video densitometry by transmission measurements on blood flowing in glass microcapillaries (15–75 μm), confirmed the wavelength independence of S and s, and demonstrated the insensitivity of O_2Sat. determinations to changes in blood flow, vessel diameter, and hematocrit. The *in vitro* accuracy was 1% O_2Sat. Their technique was also applied to O_2Sat. measurements on small vessels (15–100 μm) in the hamster cheek pouch, where an accuracy of 4% O_2Sat. was achieved, limited mainly by inhomogeneities of the surrounding tissues.

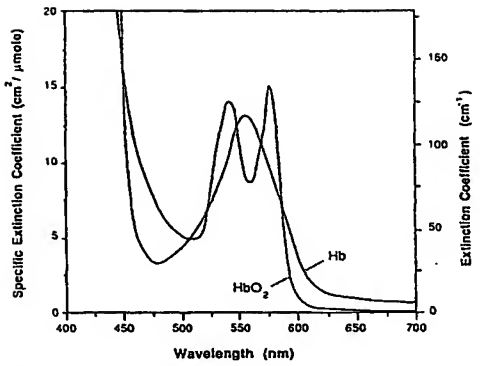

Fig. 1. Spectral variation of the specific extinction coefficients (left scale) of oxygenated hemoglobin (HbO_2) and deoxygenated hemoglobin (Hb). Data are from van Assendelft.[14] The extinction coefficients (right scale) were calculated for a total hemoglobin concentration of 15 g/100 mliter or 8.98 μmole/mliter.

B. Use in Retinal Vessel Oximetry

A retinal vessel, located in front of the fundus background (pigmented epithelium and choroid), is not accessible for transmission measurements. Instead, the light intensity V_λ reflected at the vessel is compared with the light intensity B_λ reflected in the surrounding fundus background. Vessel transmittance T_λ and density D_λ are then defined as

$$T_\lambda = V_\lambda/B_\lambda \text{ and } D_\lambda = -\log(T_\lambda). \tag{3}$$

This definition does not explicitly imply that the reflection at the vessel represents only light that was transmitted through the blood column, reflected by the underlying fundus, and retransmitted through the column to constitute V_λ. Indeed, several other light paths, involving single transmission through the blood column, are likely to contribute to V_λ. Fundus illumination is generally achieved through the peripheral parts of the pupil; thus angles of incidence at the fundus can be as high as 9°. Thus a fraction of light incident in the close vicinity of the vessel can be reflected directly through the blood column. (The reflecting layers are ~200 μm or more behind the retinal vessels.) Furthermore, light incident near the vessel will diffuse laterally in the choroidal layers and be reflected toward the blood column to contribute to V_λ by single transmission. Thus the path length distribution will depend partially on the reflection properties of the fundus background, which is known to be partially diffuse and specular.[18]

1. *In Vitro Study of the D-E Characteristic*

To investigate the nature of the D-E characteristic in the particular situation of retinal vessels, we performed the following *in vitro* experiments. Blood col-

umn densities were measured at different wavelengths for whole blood flowing through a glass capillary (100-μm i.d.), positioned against a diffuse or specular reflector. The capillary was illuminated with collimated monochromatic light (6-nm halfwidth) from a monochromator and xenon arc lamp. Specular reflections at the glass–air and glass–blood interfaces were minimized by using an angle of incidence of 10° in the plane of the capillary. The capillary was imaged with an $f/16$ lens on a 1-D optical multichannel analyzer (Princeton Applied Research) that recorded the reflection profile of the capillary and its surrounding background. Seven blood samples from three nonsmoking donors were drawn on heparin. The blood was centrifuged and washed 3 times, and the RBCs were diluted in buffered saline solution to a hematocrit of ~50%. The blood was then fully oxygenated, and O_2Sat., saturation of carboxyhemoglobin, and total hemoglobin concentration C were measured with a CO oximeter (Instrumentation Laboratories type 182). Carboxyhemoglobin saturation was <1.5% in all cases, and C varied between 14.5 and 16.0 g/100 mliter. The blood was circulated in the capillary by a syringe pump at a speed of 3 cm/s. For each sample, measurements were made at twelve different wavelengths, and the densities were calculated with Eq. (3). The densities were corrected for a glare factor of 2.5% in the optical system. That factor was calculated from density measurements (at 575 nm) of the capillary filled with saturated Evan's Blue dye, which has an extinction coefficient (~1200 cm^{-1}) that can be considered infinite compared with that of blood (140 cm^{-1}). The specific extinction coefficients E_λ at all wavelengths were calculated from Eq. (1), using averaged specific extinction coefficients (see Sec. III.D), and the extinction coefficient $C.E_\lambda$ (in cm^{-1}) was computed for each sample.

Figure 2 shows a nonlinear increase of the density at low extinctions and a quasilinear variation for extinction coefficients larger than 40 cm^{-1} or for wavelengths between 510 and 590 nm. Within the experimental error, no systematic deviation from linearity of the D-E characteristic could be demonstrated in the 510–590-nm range. The fitted value for the product $s.d$ was 73 μm in the case of the diffuse reflector. When the measurements were repeated using a specularly reflecting background (a mirror), considerable difficulties arose because of the criticality of mirror alignment and refraction effects at the capillary walls. Nevertheless, the results for two blood samples also showed a quasi-linear relationship but with larger densities and a marked reduction of $s.d$, which was ~40 μm.

2. *Oximetry of Retinal Vessels: Assumptions and Algorithms*

For retinal vessels, we assume, in analogy to Eq. (2) and on the basis of the results of the *in vitro* experiments, that the relationship between vessel density D_λ and extinction E_λ can be described by

$$D_\lambda = \alpha + \beta \cdot (E_{r,\lambda} + \Delta\lambda \cdot O_2\text{Sat.}), \quad (4)$$

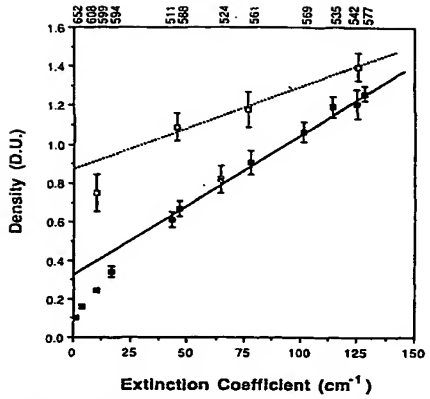

Fig. 2. Variation of blood column density vs extinction coefficient for oxygenated blood flowing through a 100-μm glass capillary located in front of a diffuse (filled squares) or specular (open squares) reflector. For the diffuse reflector data, each point is the mean of measurements on seven blood samples and corresponds to the wavelength given at the top. Error bars represent ± SD. Error bars for the extinction coefficients were omitted for clarity (the coefficient of variation was ~3.6% for all green wavelengths, increasing to 7% at 650 nm). Least-squares fit to Eq. (2) of the data in the 510–590-nm wavelength range (solid line) yielded S = 0.325 D.U. and $s.d.$ = 0.0073 cm (r^2 = 0.992, $p < 0.0001$). Least-squares fit of the same data to a second-degree equation revealed a slight but not significant (p = 0.19) negative curvature. For the specular reflector data, each point is the mean of measurements on two blood samples made at only four wavelengths. Least-squares fit to Eq. (2) of the data for the three shorter wavelengths (interrupted line) yielded S = 0.88 D.U. and $s.d.$ = 0.0040 cm (r^2 = 0.98, $p < 0.05$).

where α and β are assumed to be wavelength-independent factors. It is also assumed that reflections originating anterior to the blood column are minimal. Such reflections would cause the D-E characteristic to acquire a negative curvature with a reduction in density and slope for all extinctions. In essence, Eq. (4) must thus be considered as a linear (first-degree) approximation of the D-E characteristic, valid in a narrow range of extinction coefficients, as illustrated by the D-E line in Fig. 3(a).

The selection of the spectral range for oximetry of retinal vessels is critical. Wavelengths shorter than 500 nm are adversely affected by light scattering in the ocular media and vessel walls,[19] by low fundus reflectance,[20,21] and by stringent light safety considerations. For wavelengths longer than 600 nm, vessel detection is difficult because of low blood column contrast (Fig. 2) and nonuniformity of fundus background reflection.[19] Furthermore, reflection by the blood column in red light[22] lowers the measured density and introduces an error. We have chosen the 550–590-nm spectral range as a compromise and also because the hemoglobin spectra (Fig. 1) in that range contain appropriate wavelengths for oximetry. We use two isobestic wavelengths at 569 and 586 nm and the 558-nm wavelength as the measuring wavelength, where extinction changes are most sensitively affected by changes in O_2Sat. [Fig. 3(b)].

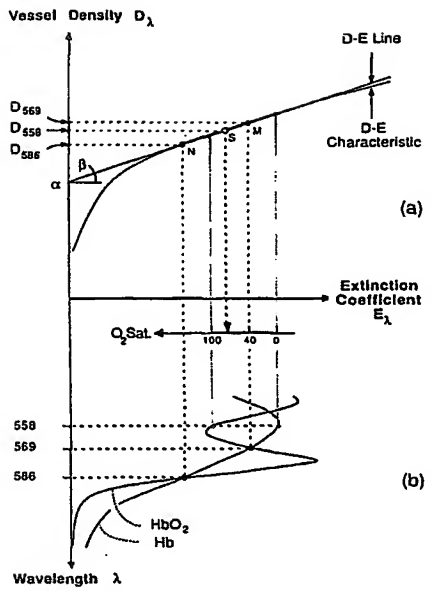

Fig. 3. Interrelationship between the measured vessel density D_λ, the specific extinction coefficient E_λ, and the wavelength λ. The two diagrams represent (a) the *D-E* characteristic and the *D-E* line [Eq. (4)] (the latter is a linear approximation of the *D-E* characteristic in the narrow range of extinction coefficients used) and (b) a section of the absorption spectra (Fig. 1) for oxygenated (HbO_2) and deoxygenated (Hb) hemoglobin. A graphic solution of the three-wavelength method is represented by the interrupted lines. Vessel density measurements D_{569} and D_{586} at the two isobestic wavelengths with known extinction coefficients $E_{r,569}$ and $E_{r,586}$ ($\Delta_{569} = \Delta_{586} = 0$) define the points *M* and *N* of the *D-E* line (intercept α and slope β). The extinction coefficient E_{558} is not known but varies between extreme values $E_{o,558}$ (O_2Sat. = 100%) and $E_{r,558}$ (O_2Sat. = 0%). The third density measurement D_{558} gives point *S* on the *D-E* line and hence the unknown extinction value. O_2Sat. is derived by linear interpolation, which is represented by the small O_2Sat. scale along the E_λ axis. The slope β of the *D-E* line reflects the sensitivity for detection of changes in hemoglobin absorption.

Density measurements of retinal vessels are made at the three selected wavelengths. Figure 3 gives a graphic solution for O_2Sat. determination, which illustrates the concepts of the method. In practice, three simultaneous equations, similar to Eq. (4) (with λ = 558, 569, and 586 nm), are solved for O_2Sat. (in percent), using RP as an operator:

$$\mathrm{RP} = \frac{D_{569} - D_{558}}{D_{569} - D_{586}} = \frac{\log(T_{558}/T_{569})}{\log(T_{586}/T_{569})}, \tag{5}$$

$$O_2\mathrm{Sat.} = 100 \cdot \frac{(E_{r,569} - E_{r,558}) + (E_{r,586} - E_{r,569}) \cdot \mathrm{RP}}{(\Delta_{558} - \Delta_{569}) + (\Delta_{569} - \Delta_{586}) \cdot \mathrm{RP}}, \tag{6}$$

with $\Delta_\lambda = E_{o,\lambda} - E_{r,\lambda}$. The two other unknowns α and β are also easily derived. The 569- and 586-nm wavelengths are nominally isobestic ($\Delta_{569} = \Delta_{586} = 0$), and O_2Sat. would then be linearly related to RP. In practice, because of manufacturing tolerances of the interference filters and the effects of the finite halfwidth of the filters (see Sec. III.D), the coefficients Δ_{569} and Δ_{586} are small, and the relationship is quasi-linear. The

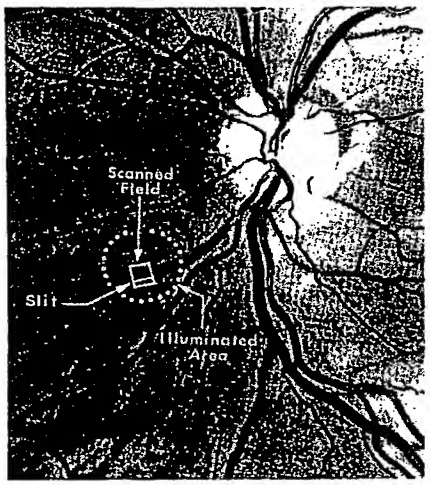

Fig. 4. Fundus photograph of a normal subject illustrating the size of the scanned field around a retinal vein within the restricted illumination area used during oximetry. Retinal veins are larger and darker than arteries, and both show an irregular linear reflex, which is caused by specular reflection at the inner limiting membrane of the retina. In general, the optic disk is ~1800 μm in diameter, and the diameter of the largest vessels is ~150–200 μm for veins and 120–140 μm for arteries.

difference $D_{569} - D_{586}$ must be large so that no large uncertainty is introduced in the calculation of RP [Eq. (5)]. This is achieved by the choice of 569 and 586 nm, which have large and low extinctions, respectively [Fig. 3(b)]. The choice of 558 nm as the O_2Sat.-sensitive wavelength corresponds, for the expected physiological range of 40–100% O_2Sat., to a narrower range of extinction coefficients than if the 575-nm wavelength were used. This, together with the narrow spectral span encompassed by the three wavelengths, helps in ensuring the approximation of Eq. (4) and the wavelength independence of the parameters α and β. For O_2Sat. of ~40%, $E_{569} = E_{558}$, and RP = 0. The measurement is then not influenced by the density determination at 586 nm, and the lowest errors that can be expected for O_2Sat. are around 40%.

III. Retinal Vessel Oximeter

Oxygen saturation (O_2Sat.) measurement involves determining vessel density at three wavelengths. This is accomplished by a 1-D scan across the vessel as illustrated in Fig. 4, providing information on the relative reflectance of the vessel and surrounding fundus background. This measurement must be made despite eye movements, involuntary blinks, and the presence of multiple vessels in the scanned field and in light conditions limited by safety considerations. As a consequence, rapid data acquisition, pattern recognition, and signal averaging are imperative. In addition to the three wavelengths needed for oximetry, the RVO accommodates a fourth wavelength, allowing for further experimental studies in oximetry and other reflectometry applications. A schematic diagram of the RVO is given in Fig. 5. The system consists of a

modified Zeiss fundus camera, a vessel scanner attachment, electronic circuits and interface, and a 6502 microprocessor (Apple computer type II+) for signal analysis.

A. Optical System

Illumination is provided by a 100-W tungsten halogen lamp L (Sylvania, FCR), powered by a stabilized current supply, and a heat filter J. The four interference filters (Spectrotech, Inc.) are mounted on a filter wheel W, driven by a synchronous motor M. The 558-, 569-, and 586-nm filters have halfwidths of 7–8 nm and peak transmissions of 65–80%, and their sidebands are suppressed by a common blocking filter K (540–600-nm transmission). Spectral calibration of the entire system will be presented in Sec. III.D. An aperture A, located in a plane conjugate to the retina, restricts the illuminated retinal field to a circular area ~1500 μm in diameter (~5°). Retinal irradiances never exceed 5 mW cm^{-2}, which determines in regard to safe ocular exposures a maximum permissible exposure time of 6 min.[23]

The vessel of interest is brought into the illuminated area by aligning the camera and directing the gaze of the patient's eyes by means of a fixation target for the eye not under examination. An image of the vessel and surrounding retinal field is formed by the optical system of the camera (× 2.7 for an emmetropic eye) in the plane of a reticule T. The operator focuses the retinal image on the reticule and rotates the vessel scanner, mounted on the camera by means of a concentric ball-bearing R, around the camera axis so that the vessel axis is aligned with the reticule. A second retinal image is formed by the beam splitter B (reflectance: 90%) on a field aperture F. The secondary beam splitter reflection is always superimposed on the primary reflection. The image in F is further magnified (× 3.9) by a lens Q to the plane of the detecting slit S with deflection by the mirror of a galvanometric optical scanner G (General Scanning G606). The scanner location is conjugated to the entrance pupil of the optical system. The slit width is adjusted to be about one-fifth of the retinal vessel diameter, whereas slit height is generally 2–3 times the diameter. With the vessel aligned to the reticule T, its image in the detecting plane is then parallel to the slit and is displaced by the scanner in a direction perpendicular to the slit. The length of fundus area scanned is ~530 μm (1.8°). The light sampled by the slit is detected by a RCA 4526 ten-stage photomultiplier (PMT) with an S-17 photocathode (peak sensitivity, around 550 nm).

B. Electronics and Interface

All timing and controls of the system are derived from a 200-kHz crystal-controlled master clock (Fig. 5). A circuit based on resistor-weighted summation and nonrecursive digital filtering[24] is used to generate an eight-level approximation of a 48.83-Hz sine wave. This signal is smoothed and amplified and drives the synchronous motor M (Hurst, MB) and the filter wheel at 1465 rpm. A timing diagram of the principal events

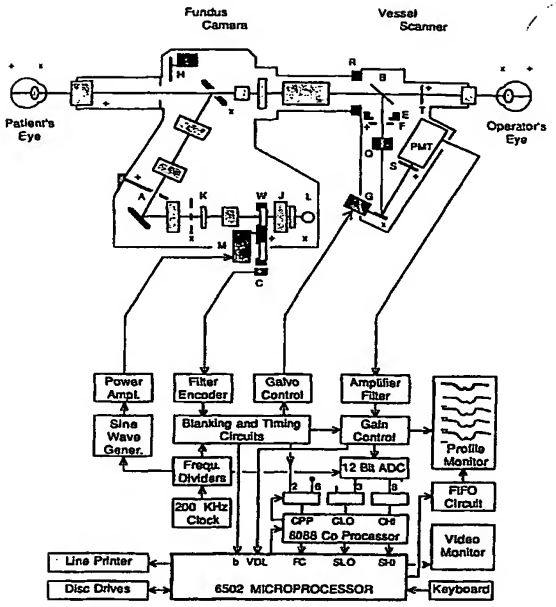

Fig. 5. Schematic diagram of the optics and electronics of the retinal vessel oximeter system. The orientation of the vessel scanner is drawn for the case of a vertically oriented retinal vessel (in the plane of the drawing). The symbol × refers to planes conjugated with the entrance pupil of the optical system (which is adjusted to be in the patient's pupil) and the symbol + to planes conjugated with the patient's retina. Unlabeled components represent lens systems (light shading) or other optical components of the Zeiss fundus camera. See text for explanation of symbols.

is shown in Fig. 6. Signals from sensors C, detecting the position of the different filters, are used in combination with the basic clock to generate a blanking signal b and all timing and synchronizing signals for galvanometer scanning and PMT signal processing. D–A conversion of counted 25-kHz pulses within the unblanked interval generates the ramp signal r, which drives the galvanometer in synchrony with the presence of a filter in the light beam. The photomultiplier signal is preamplified, filtered by a low-pass filter (1400-Hz cutoff), multiplexed to provide individual gain control for each wavelength channel, and zeroed during flyback of the scanner by the blanking signal b. The resulting signal v thus represents in sequence the reflection profiles of vessel and surrounding fundus background at successive wavelengths. These profiles are displayed on the profile monitor (Fig. 5) for inspection by the operator. Each scan is converted into an 11-bit digital signal of 192 channels using an A–D converter (Micronetworks, 5216) at a rate of 20 μs/conversion. Each channel thus corresponds with a distance of 2.76 μm at the retina. The converted signal channels are immediately transferred via two tri-state buffers into an 8088 coprocessor (ALF Products, Inc.) to provide temporary storage of the vessel profile while it is being acquired. The 8 most significant bits of the signal are stored in an array *CHI* in the coprocessor and the 3 least significant bits in an array *CLO*. A

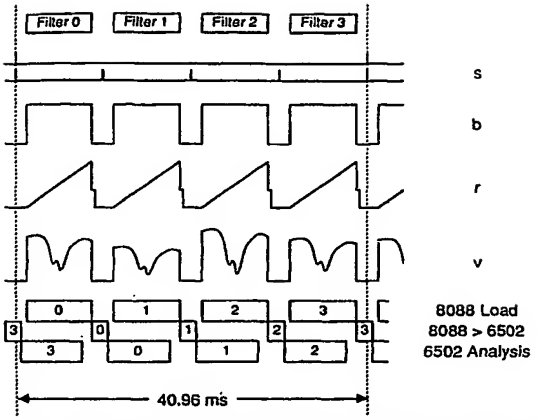

Fig. 6. Timing diagram of various signals in relation to the presence of the four wavelength filters (0, 1, 2, 3 at top) in the illumination beam: *s*, the filter wheel sensors signals; *b*, the blanking signal; *r*, the ramp signal driving the galvanometric scanner; and *v*, the vessel profiles at successive wavelengths. The step decrease of the ramp signal during flyback minimizes oscillations of the mirror. The sequence of data acquisition in the 8088 coprocessor, transfer to the 6502 microprocessor, and analysis of the different wavelength scans are indicated by the bars. After scan analysis is completed, the 6502 microprocessor waits until the acquisition of the next wavelength is completed.

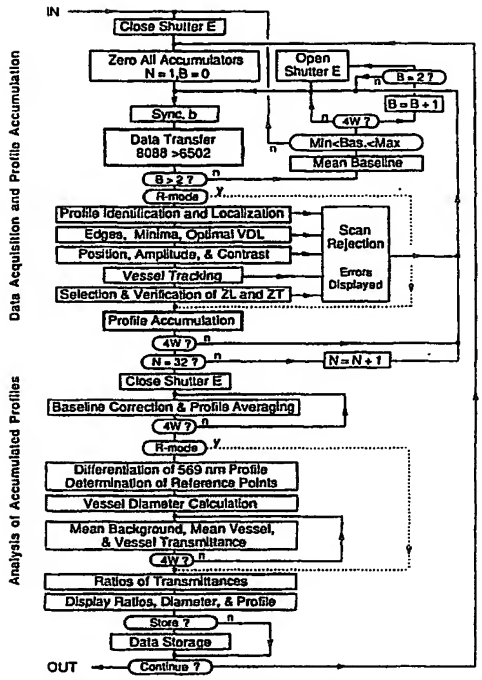

Fig. 7. Flow chart of the computer program of the 6502 microprocessor. The program consists of a sequence of data acquisition and accumulation of the four wavelength scans and a sequence of detailed analysis of the accumulated profiles. *B* and *N* are base line and accumulation counters, respectively. (4*W*?) checks that all four wavelengths have undergone a particular operation. The interrupted lines refer to operation of the RVO in the reflectance mode (*R* mode). The symbols *y* and *n* indicate a yes or no answer to a particular question.

third input *CPP*, interrogated after each scan, handles the 2-bit filter code and a 6-bit input for physiological data (such as heart pulse or respiration volume) that are recorded in some experiments. The data arrays stored in the 8088 coprocessor are transferred in 1.6 ms into the 6502 processor in arrays *SLO* and *SHI* during the initial part of the blanking. Similarly, filter code and other signals are also stored in memory. The 192-channel vessel profile (multiplied by 2^5) is thus stored in the 2-byte array *SLO* and *SHI*. This profile is analyzed by the 6502 during acquisition of the next wavelength scan (Fig. 6, bottom).

C. Microcomputer and Data Analysis

A flow chart of the microprocessor machine language program is given in Fig. 7. It occupies about 8K of memory and uses floating points subroutines stored in ROM of the system's monitor. Various functions of the microprocessor are synchronized to the above-described events by the blanking signal.

1. Data Acquisition and Profile Accumulation

Each data acquisition sequence involves an accumulation of thirty-two vessel profiles at each of the four wavelengths. Each sequence begins with the recording of two base line scans for each wavelength by closing the shutter *E* (Uniblitz type 23X) located in the vessel scanner attachment (Fig. 5). The average base line signal must be between 5 and 10% of full scale, or an error will prompt the operator to adjust the amplifier offset. This is followed by the acquisition and analysis of the vessel profile, which, except for the actual accumulation, is performed on the array *SHI* (8 most significant bits).

The analysis of the stored profile consists in identifying and localizing the vessel of interest. Eye movements cause the vessel profile to shift continuously in the scanned field and even to disappear from the field during large eye movements. Other complicating factors are nonuniform background reflectance which could be mistaken for a vessel, varying overall signal intensity, and the presence of a second vessel in the scanned field as retinal arteries and veins often run parallel to each other (Fig. 4). Figure 8(a) shows a typical vessel profile as stored in *SHI*. The positions of the intercepts of a vessel detection level (VDL) with the vessel and/or the background of the profile are determined. At the beginning of an accumulation, VDL for each wavelength is set at $\frac{7}{8}$ of the average intensity of the entire scan (calculated by integration of the analog signal), and its level is then automatically adjusted (see later). The operator selects one of two modes, leading *L* or trailing *T*, depending on the position of the vessel of interest with respect to other features in the scan. The number of intercepts, the signal amplitude relative to VDL at the leading or trailing edge of the scan, and the selected mode are used in an algorithm to accept or reject all possible patterns and configurations of the scan signal, as detailed in Fig. 8(b).

The center of the identified vessel is determined as the midpoint between its intercepts and VDL [Fig. 8(a)]. A differentiation routine searches for the vessel minima v and the vessel edges b (slope < preset value). The half-height level (HHL) is computed as the average between the smallest b and highest v. VDL is then increased or decreased to approach HHL, and this value is stored for use in the next scan of the same wavelength. This ensures that VDL adjusts itself automatically to intercept the profile where its slopes are the highest and hence where determination of the center C is most accurate. Several criteria are used to reject profiles that are inappropriate for analysis: extreme position of the vessel center, poor vessel contrast (b-v < b/8), vessel width at HHL too small (<50 μm) or large (>200 μm), too low or high signal.

The system incorporates a 1-D vessel tracking system, which greatly facilitates data acquisition in the presence of eye movements. This system operates independently of the above position determination and can be bypassed if needed. The difference between a preset vessel center position and the detected vessel center C is used to generate an offset for the galvanometric scanner causing the vessel in the next scan to be centered on the preset position. The offset is implemented at the start of the next scan, and thus one scan after the position error was detected. The scanner locks itself on the vessel, allowing scanning over a small distance (530 μm) around the vessel with good spatial resolution, while the vessel drifts over a large distance in the illuminated area (1500 μm in diameter).

Using the vessel center C as registration, a fixed number of channels at either side of the center are selected for accumulation, so that $ZL + ZT = 144$ channels [Fig. 8(a)]. The operator adjusts the extent of background at the leading or trailing side of the vessel to avoid other vessels or retinal features that interfere with the measurement. The tracking system facilitates adjustment of ZL and ZT, since the vessel profiles on the profile monitor remain virtually stationary despite eye movements.

The selected and registered 144 channels in SLO and SHI are then divided by 2^5 and added to a 16-bit accumulator array corresponding to the wavelength under analysis. Error-free analysis and accumulation of four successive wavelength scans cause the accumulator counter to be increased (Fig. 7). The signal accumulation is terminated after 32 scans for each wavelength (duration: 1.4 s, if no scan rejections).

2. *Analysis of Accumulated Profiles*

The data in the four accumulators are corrected for the base line contribution measured at the start of the sequence. A detailed analysis is then performed on the accumulated 569-nm profile, as shown in Fig. 8(c). The most significant byte of the 16-bit array is used. Differentiation and analysis of this profile determine first the positions SL and ST of largest slope on the vessel profile, and the vessel diameter (VD) is defined and calculated as the distance between SL and ST

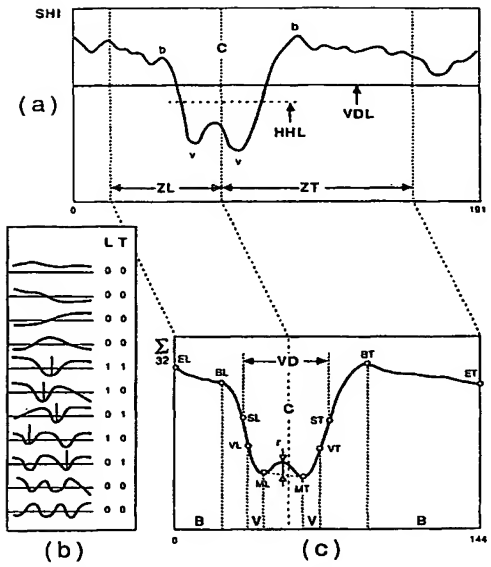

Fig. 8. (a) Typical reflection profile of a vessel as recorded in array *SHI* (192 channels). The intercepts of the VDL with the vessel profile are used to define the vessel center C midway between the intercepts. Fixed sections of the profile ZL (on the leading side of C) and ZT (on the trailing side of C) are selected for accumulation ($ZL + ZT = 144$ channels). The vessel edges b and vessel minima v, as well as the HHL, are determined for each scan. (b) Possible patterns of the recorded scan illustrating scan acceptance (1) or scan rejection (0) for the selected mode L (leading) or T (trailing). The vertical lines indicate the selected vessel. (c) Accumulated profile corresponding with the 569-nm wavelength (144 channels). EL and ET: edges of the scan; BL and BT: background edges; SL and ST: positions of maximal slope; ML and MT: vessel profile minima; VL and VT: points located at half-height between the S and M points on each side of the profile. At this and other wavelengths, background reflection is integrated in the two zones marked B and vessel reflection in the two zones marked V. Also derived from the profile analysis are the vessel diameter VD and the reflex factor ρ defined as r/mean background signal.

(scale factor of 2.76 μm/channel). The position of the edges BL and BT between the vessel and background is also defined where the slope is <1/8 of maximum slope but not farther than one VD from C. The positions of the two-vessel minima ML and MT, which generally occur for large vessels because of specular reflection at the internal limiting membrane of the retina (Fig. 4), are also determined. Points ML and MT merge in the absence of a resolved vessel reflex. Two points VL and VT are defined at half-height between SL and ML and between ST and MT, respectively. The accumulated 569-nm profile, together with all the above-defined reference points, is outputted from the microcomputer via a FIFO-based memory circuit[25] that displays the 569-nm profile on the profile monitor. This profile is updated after each analysis and helps the operator to verify adjustment of all parameters.

Mean background and vessel reflectance are then calculated at all wavelengths using the reference points defined on the 569-nm profile. Mean back-

ground is computed using floating point subroutines within the limits EL to BL and BT to ET; mean vessel reflectance is calculated within the limits VL to ML and MT to VT [Fig. 8(c)]. The limits of integration for the vessel measurement were selected to minimize the influence of the vessel reflex but also because the highest sensitivity [high value of β in Eq. (4)] was found to occur when that part of the profile was used. Vessel transmittances T_{558}, T_{569}, and T_{586} are calculated for each wavelength by using the vessel and background averages [Eq. (3)]. The ratios T_{558}/T_{569} and T_{586}/T_{569} are computed and displayed on the video monitor together with vessel diameter. The first ratio varies with O_2Sat. The second ratio varies with the slope β and hence provides a predictor for the sensitivity to hemoglobin absorption changes for the particular vessel of interest. Vessel measurements are not attempted if the ratio T_{586}/T_{569} is smaller than 1.1 (see Sec. V.A). The analysis of the accumulated data is completed in 0.2 s.

3. Data Storage and Off-Line Analysis

Each sequence of data acquisition (32 scans per wavelength) followed by analysis of the accumulated profiles is defined as one determination (total duration: 1.6 s, if no scan rejection), and these determinations are made continuously. When the appropriate options for a particular vessel have been selected, and alignments and sensitivity are optimal, the operator depresses a foot pedal, causing all data from one determination to be stored. This includes vessel diameter, vessel transmittance, and intensity of background reflection at all wavelengths, the two ratios of transmittances, reflex factor ρ [defined in Fig. 8(c)], and time of measurement (derived from an internal clock). Measurements on one vessel generally require 15 to 20 determinations or a total time of 25–35 s (no scan rejections). Each measurement is terminated by an evaluation of the relative light intensities and system sensitivities for each wavelength channel: a white reflector is inserted in a plane common to both illumination and detection in the fundus camera (at H, Fig. 5) and the light intensities measured using the reflectance mode (see Sec. III.C.4).

A detailed analysis of the stored data, which takes ~2 min to complete, is made off-line after the measurement session. O_2Sat. is calculated by means of Eqs. (5) and (6), using the average extinction coefficients derived in Sec. III.D. Mean and standard deviations of all parameters are computed for the 15 to 20 determinations that typically constitute a vessel measurement. These parameters are: O_2Sat., vessel diameter, the intercept α and slope β of the D-E line [Eq. (4), Fig. 3], the reflex factor ρ, and the relative background reflectances $R_{b,558}/R_{b,569}$ and $R_{b,586}/R_{b,569}$ (corrected for the relative signal intensities measured with the white reflector).

4. Reflectance Mode of Operation

The RVO can also operate in a reflectance mode, which parallels the data acquisition, accumulation, and analysis sequences of the oximetry mode (Fig. 7) but does not involve any vessel-related operations. The light intensities reflected by the fundus background, in areas devoid of visible retinal vessels, can thereby be measured at four wavelengths and ratios of these intensities calculated. This mode can be used in other reflectometry applications[26,27] and is also used after oximetry measurements to calibrate background reflectance measurements (see Sec. III.C.3).

D. Spectral Calibration and Algorithms for O_2Sat. Calculation

The calculation of O_2Sat. using Eq. (6) requires in addition to the operator RP derived from the measured densities [Eq. (5)], knowledge of the specific extinction coefficients, $E_{o,\lambda}(HbO_2)$ and $E_{r,\lambda}(Hb)$, and thus $\Delta_\lambda = E_{o,\lambda} - E_{r,\lambda}$. These coefficients are known from the spectral measurements of van Assendelft[14] with a spectral resolution of 0.1 nm. Since the spectral bandwidths used in the RVO are between 7 and 9 nm, it is necessary to calculate the extinction coefficients, averaged over the spectral distribution of the light transmitted by the blood column with reflection by the fundus background. Using Eq. (2), this average coefficient E_λ can be calculated by[7]

$$E_\lambda = \frac{1}{s.C.d} \cdot \log \frac{\sum R_{b,\lambda} \cdot F_\lambda \cdot 10^{-s.C.d.E'_\lambda} \cdot \Delta\lambda}{\sum R_{b,\lambda} \cdot F_\lambda \cdot \Delta\lambda}, \quad (7)$$

where $R_{b,\lambda}$ is the spectral reflectance of the fundus background, F_λ is the spectral distribution corresponding to each wavelength band, s is the scattering parameter, C is the hemoglobin concentration, d is the path length, and E'_λ is the (narrowband) extinction coefficient.[14]

The spectral distribution F_λ for each oximetry spectral band was measured for the entire optical system to include the spectral characteristics of the oximetry filters W as well as of the lamp L, heat filter J, blocking filter K, beam splitter B, optical elements, and PMT (Fig. 5). The slit assembly S was replaced by a small monochromator (PTR Optics, 0.3-nm spectral resolution), calibrated by means of standard lamps (Hg, Ne, Ar, He–Ne). An artificial eye with a barium sulfate standard reflector as fundus was used. Light intensities, averaged over the total angular extent of each filter on the filter wheel, were recorded using the reflectance mode at successive monochromator settings. The resulting spectral distributions are shown in Fig. 9, superimposed on the extinction spectra of HbO_2 and Hb. The average wavelengths, halfwidths, and tenth-widths of the three spectral bands are given in Table I.

Fundus reflectance $R_{b,\lambda}$ for different degrees of fundus pigmentation is given by a family of spectra (Fig. 9) derived from the study of the reflectance characteristics of eleven normal subjects.[21] Each spectrum is characterized by a factor of γ defined as

$$\gamma = \frac{R_{b,586}}{R_{b,569}} - 1. \quad (8)$$

The factor γ varies inversely with degree of fundus pigmentation between 0.05 (fundus of black subject)

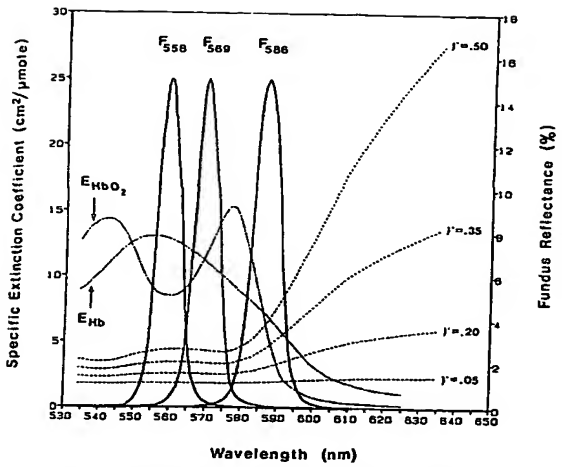

Fig. 9. Spectral distributions F_{558}, F_{569}, and F_{586} for the three spectral bands used in oximetry (solid lines, arbitrary scale). Specific extinction coefficients (dash–dotted lines, left scale) of oxygenated hemoglobin (HbO_2) and deoxygenated hemoglobin (Hb).[14] Fundus reflectance spectra[21] for different degrees of fundus pigmentations (dashed lines, right scale) with corresponding reflectance factor γ [defined by Eq. (8)] between $\gamma = 0.05$ (dark fundus) and $\gamma = 0.50$ (light fundus).

and 0.50 (albinotic fundus) and equals 0 for a spectrally uniform background. The ratio $R_{b,586}/R_{b,569}$ and hence γ, corresponding to the background of each vessel, is derived from the RVO measurement (Sec. III.C.3).

The product $s.C.d$ was evaluated with the assumption that the mean path length through the blood column equals the measured vessel diameter ($s = 1$). In other words, we assume a predominance of single transmission of light through the vessel (see Sec. II.B). The hemoglobin concentration was assumed to be $C = 8.98$ μmole/mliter (15 g/100 mliter) for all *in vivo* measurements.

To provide practical calibration algorithms that would not require recalculation of Eq. (7) for each vessel measurement, we computed average extinction coefficients for various combinations of $C.d$ and γ. For each spectral band, $E_{o,\lambda}$ and $E_{r,\lambda}$ were determined using Eq. (7) for 36 uniformly distributed combinations within the intervals $0.045 < C.d < 0.157$ μmole/cm² ($50 < d < 175$ μm) and $0 < \gamma < 0.5$ (spectrally uniform fundus to very lightly pigmented fundus). Polynomial fits of the form

$$E_\lambda = A_0 + A_1 \cdot \gamma + A_2 \cdot C.d + A_3 \cdot \gamma^2 + A_4 \cdot (C.d)^2 + A_5 \cdot \gamma \cdot C.d \quad (9)$$

were obtained for all cases ($p < 0.0001$) with statistically significant parameters A in each case. The parameters A_0 to A_5 are given in Table I. Variations in E_λ, induced by changes in γ and $C.d$, are most pronounced for the 586-nm filter, as this spectral band coincides with the rapid decrease in extinction coefficients of hemoglobin and the rapid increase in fundus reflectance (Fig. 9). Substitution of $E_{o,\lambda}$ and $E_{r,\lambda}$ in Eq. (6)

Table I. Characteristics of the Spectral Bands used for Oximetry and Parameters used in Eq. (9) for the Calculation of the Average Specific Extinction Coefficients of Hemoglobin

	569-nm filter	558-nm filter	586-nm filter
Average wavelength (nm)	569.8	559.3	586.5
Halfwidth (nm)	7.7	7.5	8.5
Tenth-width (nm)	25.3	23.6	39.6

Parameters of Eq. (9)	$E_{o,569}$	$E_{r,569}$	$E_{o,558}$	$E_{r,558}$	$E_{o,586}$	$E_{r,586}$
A_0	11.77	11.02	8.81	12.71	6.93	7.05
A_1	−0.04	−0.00	−0.02	−0.00	−1.76	−0.56
A_2	−3.20	−0.67	−0.53	−0.17	−14.66	−1.34
A_3	0.01	−0.01	0.01	0.00	0.64	0.20
A_4	−2.63	−0.94	0.74	−0.21	19.94	−0.68
A_5	−0.85	−0.25	0.03	0.00	2.16	−0.36

$E_{o,\lambda}$ and $E_{r,\lambda}$ are the average extinction coefficients of HbO_2 and Hb, respectively. Each extinction coefficient is calculated using Eq. (9): $E_\lambda = A_0 + A_1 \cdot \gamma + A_2 \cdot C.d + A_3 \cdot \gamma^2 + A_4 \cdot (C.d)^2 + A_5 \cdot \gamma \cdot C.d$. The extinction coefficients are in cm²/μmole, $C.d$ in μmole/cm², and γ is dimensionless.

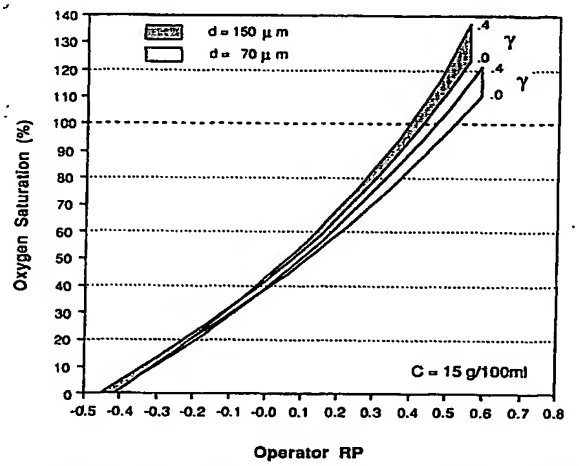

Fig. 10. Relationship of O_2Sat. and measured operator RP [Eq. (6)] for extreme values of vessel diameter (shaded areas: 70 and 150 μm) and of the reflectance factor γ (0–0.4; for a spectrally uniform background to that of a lightly pigmented fundus).

for extreme values of γ and $C.d$ gives relationships between O_2Sat. and RP depicted in Fig. 10. The effect of varying γ and $C.d$ is most pronounced for arterial O_2Sat. and decreases toward lower O_2Sat.

To summarize, O_2Sat. of blood in a vessel is calculated using Eq. (6) by substitution of the operator RP derived from the measured vessel densities for each of the three spectral bands [Eq. (5)]. The average extinction coefficients $E_{o,\lambda}$ and $E_{r,\lambda}$ [used in Eq. (6)] are determined individually for each vessel measurement by means of Eq. (9) (with the A coefficients of Table I). The product $C.d$ is calculated from the measured vessel diameter d (with the normal hemoglobin concentration $C = 8.98$ μmole/mliter for all *in vivo* measurements and the measured C for *in vitro* measurements).

The factor γ [Eq. (8)] is derived from the background reflectance ratio $R_{b,586}/R_{b,569}$ measured locally in the vicinity of each vessel (Sec. III.C.3). It is clear that the use of interference filters with narrower bandwidths or the use of a dye laser would greatly facilitate the calibration of the technique and eliminate the need for calculating the averaged extinction coefficients of hemoglobin.

IV. *In Vitro* Measurements

O_2Sat. was measured with the RVO for blood flowing through glass capillaries (50-, 100-, or 150-μm i.d.) located at the retina of a water-filled artificial eye (focal length: 22 mm). The capillary was positioned at ~200 μm from a reflecting background, whose reflection was spectrally uniform and either diffuse (white paper) or specular (finely ground aluminum surface). Those two background types were chosen because the fundus background is known to be partially diffuse and specular.[18] Blood from two nonsmoking donors was prepared as in Sec. II.B.1. The O_2Sat. of the washed blood was changed by flushing the blood samples with oxygen or nitrogen; some samples were totally deoxygenated by mixing it to excess with sodium dithionite. The O_2Sat., total hemoglobin concentration C, and carboxyhemoglobin saturation were measured with a CO oximeter (Instrumentation Laboratories type 282). Carboxyhemoglobin saturation was <1.0% in all cases, and C varied between 11 and 20 g/100 mliter. The blood, stored in a gastight syringe, was circulated in the capillary by a syringe pump at blood flows of 1–90 μliter/min, and measurements were made with the RVO. Refraction effects at the water–glass and glass–blood interfaces caused reflection irregularities at the edges of the capillary profile, which necessitated locating the points BL and BT farther from C [Fig. 8(c)] than in the method described in Sec. III.C.2. The measured capillary densities were corrected for a glare factor of 2.7% (determined as in Sec. II.B.1). The O_2Sat. was calculated using the algorithms described in Sec. III.D. The factor γ equaled 0 (uniform background reflectance), and $C.d$ was calculated for each experiment from the measured hemoglobin concentration and the internal diameter of the capillary. The correction for system glare resulted in an increase of ~1.5% O_2Sat. at high O_2Sat. and a decrease of ~2% at low O_2Sat.

Figure 11(a) shows the RVO output recording for O_2Sat., for a 100-μm capillary in front of a diffuse reflector, and for blood samples oxygenated at different levels. For all samples in this study (n = 118), standard deviations for the 10 to 15 determinations that constitute the measurement of a sample were on average 1.6 and 5.6% O_2Sat. for the diffuse and specular reflector, respectively. There was a trend for the standard deviation to increase with mean O_2Sat. (p = 0.1 and $p < 0.02$, respectively), but there was no significant dependence on $C.d$.

No statistically significant dependence of the measured O_2Sat. on blood flow, for blood flows between 1 and 90 μliter/min, could be detected for each capillary

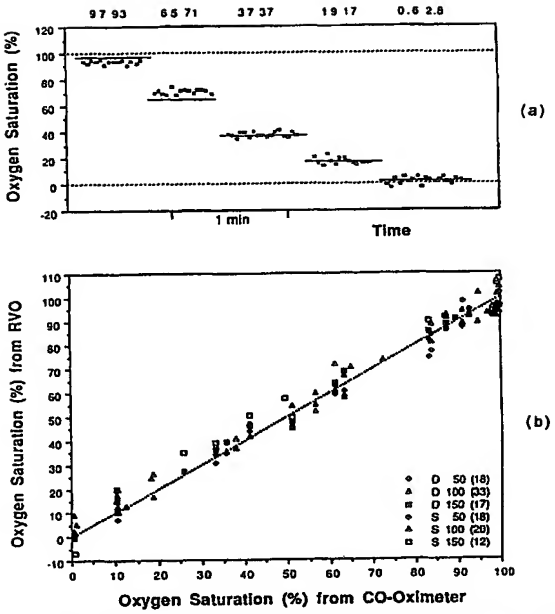

Fig. 11. (a) RVO output traces of O_2Sat. measurements for blood flowing through a 100-μm glass capillary positioned in front of a diffuse background. Each point represents one determination or 1.6 s of data acquisition and analysis. The traces correspond to five blood samples (from one subject) oxygenated at different levels and also measured by standardized CO oximetry. The O_2Sat. measured with the CO oximeter is shown by lines and given in bold type at the top of each trace, whereas values given in plain type correspond to the RVO measurement, which is the average of 10–15 determinations (SD: 1.3–2.4% O_2Sat.). (b) Comparison of O_2Sat. measured by the RVO and the CO oximeter for various combinations of capillary diameter and background reflector. The key indicates, for each symbol, the nature of the background reflector (D, diffuse; S, specular), the diameter in micrometers, and the number of blood samples measured (in parentheses). The dotted line shows the equality of O_2Sat. measured by the two methods.

diameter. A blood flow of 7 μliter/min was, therefore, used for all experiments and all capillary diameters.

The comparison of O_2Sat. measured with the RVO and those determined with the CO oximeter is shown in Fig. 11(b) for all 118 combinations of blood samples, capillary diameter, and background reflector. The results show good general correspondence of the RVO measurements with the CO oximeter determinations. Multiple regression analysis indicated the following relationship between O_2Sat.$_{RVO}$ determined by the RVO and O_2Sat.$_{CO}$ determined by the CO oximeter:

$$O_2\text{Sat.}_{RVO} = (-0.8 + 4.1 \cdot I_{br} + 33 \cdot C.d) + 0.95 \cdot O_2\text{Sat.}_{CO}, \quad (10)$$

$$p < 0.0001 \qquad p < 0.008 \qquad p < 0.0001$$

where the indicator variable I_{br} = 0 or 1 for a diffuse or specular background, respectively. The statistical significance of each coefficient is indicated, and the regression had a standard deviation of 4.3% O_2Sat. (r^2 = 0.98, $p < 0.0001$). No statistically significant effect of the background type I_{br} could be demonstrated on the coefficient of either $C.d$ or O_2Sat.$_{CO}$ (slope). Thus O_2Sat. determined with the specular background was

on average 4.1% O_2Sat. higher than those determined with the diffuse background. The dependence of O_2Sat. on $C.d$ is equivalent to an increase of 0.3% O_2Sat. for every 10-μm increase in capillary diameter. Considering all the data in a pooled fashion indicated that for $O_2Sat._{CO}$ of 100%, the measured $O_2Sat._{RVO}$ was 99.2% O_2Sat. with a 95% confidence interval of ±1.6% O_2Sat. For $O_2Sat._{CO}$ of 0%, the measured $O_2Sat._{RVO}$ was 3.8% O_2Sat. with a 95% confidence interval of ±2.1% O_2Sat. The measured $O_2Sat._{RVO}$ was significantly higher than the CO oximeter values for saturation between 0 and 50% (mean difference 3.8 and 1.4% O_2Sat., respectively), but no significant differences existed between 50 and 100%.

For the measurements on the diffuse background, and for capillaries with diameters of 50-, 100-, and 150-μm diameter, the mean intercept α of the D-E line [Eq. (4)] was 0.18, 0.34, and 0.46 D.U., and the mean slope β was 0.036, 0.063, and 0.080 μmole/cm^2, respectively. For the measurements on the specularly reflecting background, the mean intercept α was 0.58, 0.99, and 1.13 D.U., and the mean slope β was 0.33, 0.04, and 0.07 μmole/cm^2, respectively. This confirms the findings of the preliminary *in vitro* experiments (Fig. 2) and indicates higher densities and lower sensitivity to changes in hemoglobin absorption (slope β, Fig. 3) when the background is a specular reflector than when it is diffuse. This also explains partially the higher variability of the measurements on the specular than the diffuse background.

In conclusion, the three-wavelength oximetry method provides reasonable agreement with standardized CO oximetry, despite large changes in the vessel diameter, nature of the background reflection, and blood flow.

V. *In Vivo* Measurements

The subject's pupil is dilated to a minimum diameter of 6 mm. The vessel of interest is aligned using a fixation target for the fellow eye on the optical axis of the instrument. After focusing and selection of vessel detection modes, the measurements are initiated. The subject is asked to blink frequently to avoid poor vessel image quality (uniform corneal tear film). Subjects rarely complain about the light levels but are occasionally disturbed by the flicker of the colored illumination. After measurements of several vessels, the data are analyzed off-line and the results inspected. Occasionally a vessel is remeasured immediately if the results are too variable. The O_2Sat. was calculated using the algorithms described in Sec. III.D.

A. Measurements on Individual Vessels

Typical results of O_2Sat. and corresponding vessel diameter for several vessels in a normal volunteer are given in Fig. 12(a). Results of measurements monitoring changes in O_2Sat. and vessel diameter before and during hyperoxia (breathing 100% O_2) are given in Fig. 12(b) for an artery and vein of one subject.

Standard deviations for the 15 to 20 determinations that constitute a vessel measurement ranged between

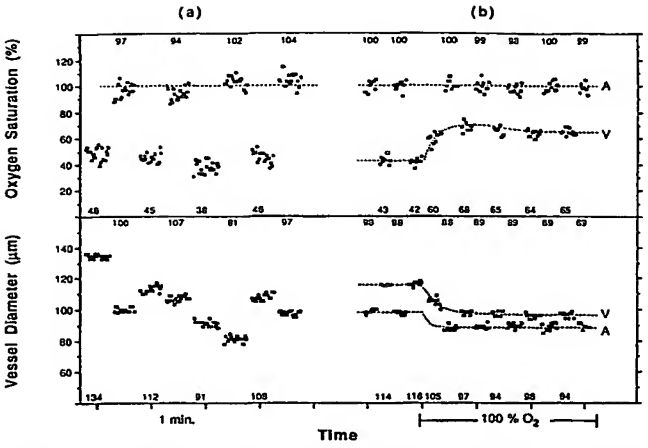

Fig. 12. (a) RVO recording showing O_2Sat. (top traces) and vessel diameter (bottom traces) for four veins and four arteries in one normal subject (age: 33). Each point represents one determination or ~1.6–3 s of data acquisition and analysis. Average values for each group of determinations are given at the top of each trace for arteries and at the bottom of each trace for veins. The standard deviations for the O_2Sat. and vessel diameter measurements were 3.5 to 5.9% O_2Sat. and 1.3–2.0 μm, respectively. The reflectance factor γ ranged between 0.21 and 0.35, reflecting differences in local pigmentation of the fundus. (b) O_2Sat. and vessel diameter response to breathing 100% O_2 in one subject (age: 35). The measurements were made alternately on the artery A and on the vein V of a vascular segment, and the average results are given as in (a). The standard deviations for the O_2Sat. and vessel diameter measurements were 2.4–4.3% O_2Sat. and 0.5–2.3 μm, respectively (excluding the venous data during the rapid change). The results show no detectable change in arterial O_2Sat. but a substantial increase in venous O_2Sat. (from ~42 to 65 O_2Sat.). Pronounced vasoconstriction of both the artery (by ~10%) and the vein (by ~14%) is observed. The factor γ was ~0.15 for the fundus background at both vessels. O_2Sat. calculations took the changes in vessel diameter into account [Eq. (9)].

1 and 14% O_2Sat. (85 arteries and 102 veins) and were found to be on average 5.7% O_2Sat. for arteries and 4.8% O_2Sat. for veins (significantly lower than for arteries, $p < 0.002$). The 95% confidence intervals associated with the measurement are on average ±3.4 and ±2.9% O_2Sat. for arteries and veins, respectively. The standard deviation for arterial and venous diameter measurements, expressed in percent of their mean diameter, was on average 1.8%.

Several factors, or combinations of factors, were found to have an adverse effect on the variability of the O_2Sat. measurement: eye movement; high degree of fundus pigmentation (less available light); very low degree of pigmentation (nonuniform fundus background); high and irregular vessel reflex (Fig. 4); ocular media turbidity; and accidented retinal topography (such as in the immediate vicinity of the optic nerve head). Most of these factors are generally associated with low values for β, the slope of the D-E line [Fig. 3, Eq. (4)]. The denominator of the expression for RP [Eq. (5)] is then small, which results in uncertainties in the determination of RP and hence in O_2Sat. A strong negative correlation can indeed be demonstrated be-

tween the standard deviation of the measurement and the slope β for both arteries and veins ($p < 0.0001$, in both cases). For this reason, we are rejecting any measurement in which $\beta < 0.006$ μmole/cm^2, as this generally corresponds with standard deviations larger than ~10% O_2Sat. This is also the basis for our criterion for nonmeasurement used prior to data acquisition on a particular vessel ($T_{586}/T_{569} < 1.1$, Sec. III.C.2).

A source of variability inherent to the RVO technique may be the influence of the cardiac cycle, which causes pulsation in the reflectance of the fundus background,[28] in the vessel caliber,[29] and, therefore, in the vessel density. Since the RVO is not synchronized with the cardiac pulse, and since data are accumulated during 1.4 s (or more, if scan rejections occur), one obtains vessel diameters and densities averaged asynchronously over 1.5 or more cardiac cycles, and this could contribute to the variability of successive determinations. Hill and Crabtree[29] showed that the diameter of arteries and veins pulsate with the cardiac cycle by ±2–6% of their mean diameter. Using the largest figure of 6%, one can estimate from the *in vitro* observed dependence of O_2Sat. on diameter (0.03% O_2Sat./μm; see Sec. IV), that in the case of a 150-μm vessel, a difference of $2 \times 0.06 \times 150 \times 0.03$, or 0.5% O_2Sat. would be detected between scans at the diastolic and systolic extremes of the cardiac cycle. This is clearly a small effect, but other phenomena related to vessel density pulsation might influence the variability, and this will be investigated in future studies.

Reproducibility of O_2Sat. and vessel diameter measurements were evaluated for several arteries and veins, either by two measurements during the same session (with repositioning of the subject's head and realignment of the instrument) or by two measurements during different sessions (at least one week apart). For the same session O_2Sat. measurements (11 arteries and 15 veins in 8 subjects), the average standard deviation of the two measurements was 2.1% O_2Sat. (worst case, 4.2% O_2Sat.) with no significant difference between arteries and veins. The standard deviation of the vessel diameter measurements, expressed in percent of the mean of the two measurements, was on average 1.1% (worst case, 2.8%). For the different sessions O_2Sat. measurements (9 arteries and 12 veins in 6 subjects), the average standard deviation of the two measurements was 2.6% O_2Sat. (worst case, 6.3% O_2Sat.) with no significant difference between arteries and veins. The standard deviation of the vessel diameter measurements, expressed in percent of the mean of the two measurements, was 2.1% (worst case, 5.3%).

B. Measurements on Vessels in Different Subjects

Representative RVO measurements for a group of 22 normal subjects (under the age of 40) involved a total of 85 arteries and 102 veins. Vessel diameters ranged between 62 and 129 μm for arteries and 72 and 184 μm for veins. Average O_2Sat. were 98 ± 8 and 45 ± 7% O_2Sat. for arteries and veins, respectively. The factor γ was on average 0.20 and ranged between 0.08 and 0.46 for both arteries and veins. The calculated intercept α was on average 0.19 ± 0.04 D.U. for arteries and 0.30 ± 0.06 D.U. for veins (significantly higher than for arteries, $p < 0.02$). The slope β was 0.011 ± 0.003 μmole/cm^2 for arteries and 0.013 ± 0.004 μmole/cm^2 for veins (significantly higher than for arteries, $p < 0.005$). As mentioned above, these differences in β correspond with the larger standard deviations observed on average for arteries than for veins. The slopes β are smaller than those obtained *in vitro* (Sec. IV). More detailed analysis of the results in normal subjects will be presented in a later paper.

VI. Conclusions

The retinal vessel oximeter is an easy-to-use noninvasive instrument for measuring oxygen saturation of blood (O_2Sat.) in human retinal vessels. The method uses three wavelengths to compensate for the effects of light scattering by the red blood cells and to partially correct for the influence of intraocular reflections, such as ocular media scattering and vessel reflex. The system allows rapid measurements and analysis and incorporates a vessel tracking system to compensate for eye movements. In addition to O_2Sat., the RVO measures the retinal vessel diameter, which is an important parameter in the study of retinal circulation since it is associated with retinal blood flow.

Verification of the RVO method by *in vitro* experiments indicates good correspondence with a standard clinical oximetry technique. The accuracy of the O_2Sat. measurement is best in the 50–100% O_2Sat. range, but a systematic overestimation was observed for O_2Sat. lower than 50%, increasing to ~3% O_2Sat. for completely deoxygenated blood.

Oximetry on retinal vessels of normal human subjects showed average O_2Sat. to be 98 ± 8 and 45 ± 7% O_2Sat. for arteries and veins, respectively. Thus a little more than half of the oxygen carried by the arterial hemoglobin is extracted from the retinal circulation by the metabolizing retinal tissues. The range of the measured arterial O_2Sat. indicates artifactual contributions, which have been traced to the effect of ocular media and vessel wall scattering and vessel reflex and to the influence of melanin pigmentation of the choroid.[12] The range of the measured venous O_2Sat. could also indicate artifactual contributions but might also reflect physiological variations due to differences in vascular architecture and retinal location.

The present method is useful for studying changes in retinal vessel oxygenation in humans for the purpose of investigating normal physiology as well as disease.[30,31] Venous O_2Sat. measurements are particularly important, because they uniquely reflect tissue oxygenation levels and, therefore, indicate tissue hypoxia in retinal vascular diseases. Autoregulatory mechanisms, which might be themselves affected by disease, adjust the retinal blood flow rate in the vascular segments, and the net result is reflected by the arteriovenous O_2Sat. difference across those segments. Based on data presented here, disease related changes in oxygen saturation in individual vessels as small as 3–

4% O_2Sat. can be detected with this oximetry method.

The author acknowledges F. J. Rogers for the design and realization of electronic circuits, G. R. Bearse for the construction of mechanical components, and K. A. Fitch for expert assistance throughout this work. Special thanks are due to G. T. Feke, K. Pflibsen, and A. Garsd for numerous discussions and suggestions.

This work was supported by grant EY02094 from the National Eye Institute, National Institutes of Health, Bethesda, MD, and by generous support from the Walters Family Foundation, Manhasset, NY.

References

1. J. B. Hickham and R. Frayser, "A Photographic Method for Measuring the Mean Retinal Circulation Time Using Fluorescein," Invest. Ophthalmol. 4, 876 (1965).
2. C. E. Riva, G. T. Feke, B. Eberli, and V. Benary, "Bidirectional LDV System for Absolute Measurement of Blood Speed in Retinal Vessels," Appl. Opt. 18, 2301 (1979).
3. G. T. Feke, D. G. Goger, H. Tagawa, and F. C. Delori, "Laser Doppler Technique for Absolute Measurement of Blood Speed in Retinal Vessels," IEEE Trans. Biomed. Eng. BE-34, 673 (1987).
4. J. B. Hickham, R. Frayser, and J. C. Ross, "A Study of Retinal Venous Blood Oxygen Saturation in Human Subjects by Photographic Means," Circulation 27, 375 (1963).
5. J. B. Hickham and R. Frayser, "Studies of the Retinal Circulation in Man: Observation of Vessel Diameter, Arteriovenous Oxygen Saturation Difference, and Mean Circulation Time," Circulation 33, 302 (1966).
6. R. A. Laing, A. J. Cohen, and E. Friedman, "Development of Clinically Useful Methods of Estimating Choroidal and Retinal Blood Flow," Final Report, contract NIH-NEI 711-2513, National Eye Institute, National Institutes of Health, Bethesda, MD (1974).
7. A. J. Cohen and R. A. Laing, "Multiple Scattering Analysis of Retinal Blood Oximetry," IEEE Trans. Biomed. Eng. BE-23, 391 (1986).
8. R. A. Laing, A. J. Cohen, and E. Friedman, "Photographic Measurements of Retinal Blood Oxygen Saturation: Falling Saturation Rabbit Experiments," Invest. Ophthalmol. 14, 606 (1975).
9. H. J. Klose, E. Volger, H. Brechtelsbauer, and H. Schmid-Schonbein, "Microrheology and Light Transmission of Blood. I. The Photometric Effects of Red Cell Aggregation and Red Cell Orientation," Pfluegers Arch. 333, 126 (1972).
10. F. C. Delori, F. J. Rogers, S. E. Bursell, and J. S. Parker, "A System for Non-Invasive Oximetry of Retinal Vessels," in *Frontiers of Engineering in Health Care, 1982. Proceedings, Fourth Annual Conference of the I.E.E.E. Engineering in Medicine and Biology Society*, A. R. Potvin and J. H. Potvin, Eds. (Institute of Electrical & Electronics Engineers, New York, 1982), p. 296.
11. F. C. Delori, J. J. Weiter, M. A. Mainster, and V. A. Flook, "Oxygen Saturation Measurements in Retinal Vessels," Invest. Ophthalmol. Visual Sci. 24, (ARVO Suppl), 13 (1983).
12. F. C. Delori, D. M. Deupree, and J. J. Weiter, "Evaluation of the Retinal Vessel Oximetry Technique," Invest. Ophthalmol. Visual Sci. 26, (ARVO Suppl), 37 (1985).
13. R. N. Pittman and B. R. Duling, "A New Method for the Measurement of Percent Oxyhemoglobin," J. Appl. Physiol. 38, 315 (1975).
14. O. W. van Assendelft, *Spectrophotometry of Hemoglobin Derivatives* (C.C. Thomas, Springfield, IL, 1970).
15. D. L. Drabkin and R. B. Singer, "Spectrophotometric Studies: VI. A Study of the Absorption Spectra of Non-Hemolyzed Erythrocytes and of Scattering of Light by Suspensions of Particles," J. Biol. Chem. 129, 739 (1939).
16. N. M. Anderson and P. Sekelj, "Light-Absorbing and Scattering Properties of Non-Hemolyzed Blood," Phys. Med. Biol. 12, 173 (1967).
17. R. N. Pittman and B. R. Duling, "Measurement of Percent Oxyhemoglobin in the Microvasculature," J. Appl. Physiol. 38, 321 (1975).
18. R. A. Weale, "Polarized Light and the Human Fundus Oculi," J. Physiol. 186, 175 (1966).
19. F. C. Delori, E. S. Gragoudas, R. Francisco, and R. C. Pruett, "Monochromatic Ophthalmology and Fundus Photography: The Normal Fundus," Arch. Ophthalmol. 95, 861 (1977).
20. D. van Norren and L. F. Tiemeijer, "Spectral Reflectance of the Human Eye," Vision Res. 26, 313 (1986).
21. F. C. Delori and K. Pflibsen, "Spectral Reflectance of the Human Ocular Fundus," (in preparation).
22. N. M. Anderson and P. Sekelj, "Reflection and Transmission of Light by Thin Films of Nonhaemolyzed Blood," Phys. Med. Biol. 12, 185 (1967).
23. F. C. Delori, J. S. Parker, and M. A. Mainster, "Light Levels in Fundus Photography and Fluorescein Angiography," Vision Res. 20, 1099 (1980).
24. P. Horowitz and W. Hill, *The Art of Electronics* (Cambridge U.P., Cambridge, 1980), p. 448.
25. F. J. Rogers and F. C. Delori, "FIFO Memory Circuit Stores Waveform Data for Monitors and Scopes," Electron. Des. 32, No. 15, 256 (1984).
26. J. Sebag, F. C. Delori, G. T. Feke, D. Goger, K. Fitch, H. Tagawa, D. Deupree, J. J. Weiter, and J. W. McMeel, "Anterior Optic Nerve Blood Flow Decreases in Clinical Neurogenic Optic Atrophy," Ophthalmology 93, 858 (1986).
27. F. C. Delori, K. P. Pflibsen, and K. Fitch, "Fundus Reflectometry Measurements of Choroidal Blood Volume," Invest. Ophthalmol. Visual Sci. 28 (ARVO Suppl), 28 (1987).
28. J. Gloster, "Fundus Oximetry," Exp. Eye Res. 6, 187 (1967).
29. D. W. Hill and A. Crabtree, "Vascular Calibers," Trans. Ophthalmol. Soc. UK 104, 107 (1984).
30. F. C. Delori, G. T. Feke, A. Yoshida, and J. J. Weiter, "Retinal Oxygen Delivery in Hyperoxia, "Invest. Ophthalmol. Visual Sci. 25 (ARVO Suppl), 8 (1984).
31. F. C. Delori, J. Sebag, G. T. Feke, and J. J. Weiter, "Oxygen Saturation of Retinal Veins in Optic Atrophy," Invest. Ophthalmol. Visual Sci. 27 (ARVO Suppl), 221 (1986).